Recovery of rare earth elements by adsorption on biochar of dead *Posidonia oceanica* leaves

Nicola Muratore, Davide Lascari, Salvatore Cataldo, Salvatore Giovanni Michele Raccuia, Gabriele Lando, Paolo Lo Meo, Vitaliano Chiodo, Susanna Maisano, Francesco Urbani, Alberto Pettignano

PII: S1002-0721(24)00381-8

DOI: https://doi.org/10.1016/j.jre.2024.11.010

Reference: JRE 1886

To appear in: *Journal of Rare Earths*

Received Date: 28 June 2024

Revised Date: 16 October 2024

Accepted Date: 8 November 2024

Please cite this article as: Muratore N, Lascari D, Cataldo S, Raccuia SGM, Lando G, Lo Meo P, Chiodo V, Maisano S, Urbani F, Pettignano A, Recovery of rare earth elements by adsorption on biochar of dead *Posidonia oceanica* leaves, *Journal of Rare Earths*, https://doi.org/10.1016/j.jre.2024.11.010.

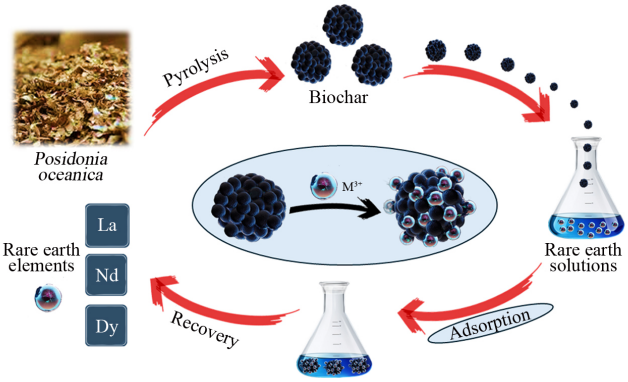

Recovery of rare earth elements by adsorption on biochar of dead *Posidonia oceanica* leaves

Nicola Muratore[a, †], Davide Lascari[a, †], Salvatore Cataldo[a], Salvatore Giovanni Michele Raccuia[b], Gabriele Lando[b], Paolo Lo Meo[c], Vitaliano Chiodo[d], Susanna Maisano[d], Francesco Urbani[d] and Alberto Pettignano[a*]

[a] Department of Physics and Chemistry – Emilio Segrè, University of Palermo, Viale delle Scienze, building 17, I-90128 Palermo, Italy
[b] Department of Chemical, Biological, Pharmaceutical and Environmental Sciences, University of Messina, Viale F. Stagno d'Alcontres 31, I-98166 Messina, Italy
[c] Department of Biological, Chemical and Pharmaceutical Sciences and Technologies (STEBICEF), University of Palermo, Viale delle Scienze, ed. 17, I-90128 Palermo, Italy
[d] CNR-ITAE institute, via Salita S. Lucia sopra Contesse 5, I-98126 Messina, Italy

☆**Foundation item:** Project supported by the Italian Ministry of Education, University and Research (MUR, PNRR - Mission 4, Component 2, Investment 1.1 - Prin 2022 Call - Directorial Decree no. 104 of 02-02-2022 "Wastezilla: Recycled waste biomass for efficient recovery of critical elements". Project codes: PRIN_2022HYH95P_001, PRIN_2022HYH95P_003)
* Corresponding author: Tel: +39-091-23897959
E-mail address: alberto.pettignano@unipa.it
† These two authors contributed equally to this work.

ABSTRACT

In this study, a pristine biochar (BCP) from dead *Posidonia oceanica* leaves, a by-product of biofuel production, and its two chemically activated forms with KOH (BBCP) and with H_3PO_4 (ABCP) were tested as new adsorbent materials for the recovery of three rare earth cations (REE), namely La^{3+}, Dy^{3+} and Nd^{3+} from aqueous solutions. The biochars were characterized through elemental analysis, nitrogen adsorption-desorption analysis, attenuated total reflectance-Fourier transform infrared (ATR-FT-IR) spectroscopy, scanning electron microscopy and energy dispersive X-ray spectroscopy (SEM-EDX), and pH_{pzc} measurements. From single batch adsorption experiments at different pH values, the pH = 5.0 was chosen as the best pH value for kinetic and isotherm adsorption studies. The effect of ionic medium on the adsorption ability of the best REE adsorbent ABCP was also evaluated by carrying out isotherm experiments in 0.1 mol/L $NaNO_3$. Inductively coupled plasma optical emission spectroscopy (ICP-OES) was used to evaluate the REE concentration in the solutions. Kinetic and isotherm data of REE adsorption were tentatively subjected to regression analysis with various kinetic and isotherm equations. The parameter values of the best fit models and characterization results were analyzed to obtain information about the adsorption mechanism. The recyclability of ABCP adsorbent was also evaluated through recycle and reuse column experiments in which 0.1 mol/L HNO_3 and EDTA were used as extractant solutions. The chemical activation processes enhance the adsorption capacity of BCP by increasing the carbonization, the specific and microporous surface area, the pore volume and, in the case of activation with H_3PO_4, introducing phosphate groups in the biochar structure. The promising REE recovery results obtained with ABCP transform the biochar from a by-product to a high value-added material. This contributes to making biofuel production a more cost-effective and environmentally-friendly process.

Keywords: rare earth elements, adsorption, recovery, biochar, *Posidonia oceanica*.

1. Introduction

Rare earth elements (REEs) are a group of 17 elements with similar chemical and physical properties. The element's group includes all the lanthanides, scandium and yttrium. Their unique properties make REEs essential in several fields. REEs are present in components of many daily used industrial products such as computers, cell phones, optical fibers, lasers, fluorescent lamps, medical equipment, electric car batteries, permanent magnets [1,2]. As long as renewable energy production is concerned, some REEs are employed as part of catalysts, in solar panels and in wind-power turbines. Moreover, they find application in agriculture as components of some fertilizers and in military applications as component of magnets in defense systems and smart bombs [1–4].

Although REEs are not "rare", they are globally distributed in low concentrations. In nature, they are found, in low percentages, only in the form of minerals from which they must be extracted with unsustainable and wasteful processes. The high amounts of reagents necessary in REEs extraction make this process non-eco-friendly [5]. In addition, these minerals, mainly xenothyme and monazite, usually contain various radioactive elements (including thorium and uranium), which must be appropriately handled [6].

The U.S. Geological Survey, Mineral Commodity Summaries 2024 estimates a worldwide mine production of REEs as large as 350000 t in 2023, 240000 t of which are produced in China. The estimate of worldwide reserves of REEs for the same year was 110000000 t, in details 44000000 t in China followed by the 22000000 and 21000000 t in Vietnam and Brazil [7]. The scenario emerging from this and previous surveys, and more generally, from recent literature, suggests that the rare earths market of the last decades has had China as its main protagonist, followed at a distance by a few other countries including Brazil and Vietnam. This great inhomogeneity in the global distribution of REEs, together with the great demand for these elements by modern industrial technology, has caused geopolitical problems in the last decades [8]. In this contest, European Community decided to include REEs in the list of critical raw materials, i.e. the list of materials with high risk of supply and considered strategic for the EU economy [9].

A possible solution to the REEs extraction and supply problems could be provided by their recovery from end-of-life electrical and electronic devices, such as cathode-ray tubes, printed circuit boards, batteries, and magnets. It is indeed recognized that electrical and electronic wastes (e-waste) have greater REEs concentrations than minerals, in particular the most precious REEs like neodymium and dysprosium. Moreover, e-waste does not contain any radioactive substances or other compounds that require proper disposal [1,2,10,11].

The REEs recovery process from solid waste, including e-waste, consists of a first phase of leaching with acids and a second phase of separation of the REEs from other metals and a subsequent separation of the REEs themselves [2,10].

Adsorption is recognized as one of the most attracting separation techniques from water phases, in particular when the employed adsorbents come from waste platforms [12–17]. Using this separation approach, the REEs present in the leaching solution can be adsorbed on the surface of a solid material with functional groups capable of selectively binding them [5,18]. Among possible adsorbents, biochars are particularly interesting. Indeed, they are low-cost carbonaceous materials produced by pyrolysis of biomasses under reducing conditions, at a temperature ranging between 350 and 700 °C. The biomasses used are generally wastes of plant origin, and the biochars are

considered themselves by-products of renewable fuel production [19–21]. The surface of biochars is rich in carboxyl, hydroxyl and carbonyl functional groups and it is reactive towards organic and inorganic species including metal cations. The latter ones can be adsorbed through different mechanisms, mainly ion exchange and complexation [22]. The pyrolysis temperatures as well as the lignin and cellulose content of the staring biomass critically affect the pore size distribution and surface area of the produced biochar [22]. The adsorption capacity of the materials can also be improved by physical or chemical activation processes.

In the present work, the adsorption of the light rare earth lanthanum and neodymium and of the heavy rare earth dysprosium onto a biochar obtained by pyrolysis of dead *Posidonia oceanica* leaves [21,23] have been studied. *Posidonia oceanica* is an endemic plant of Mediterranean Sea that forms large beds along the coasts. The dead leaves accumulate in large amounts on the Sicilian coast. It is estimated that at the end of vegetative period, a great amount of dead fragments (~10–20 t per hectare of *Posidonia oceanica* meadow) are formed and that 25% is deposited on the shorelines by the wave action. [21,24,25]. Several studies demonstrated that the pyrolysis of seaweeds and sea plants is a promising bio-fuel production process with good oil yields and high heating values [21,23]. Moreover, the large amount of beached *Posidonia oceanica* leaves on Sicilian coast and its availability for free make it the ideal biomass for the local renewable fuel production. The pristine biochar (BCP) was tested as such and after chemical activation processes with either KOH (BBCP) [13] or H_3PO_4 (ABCP) (see experimental section). BCP, either activated or not, has been already successfully used in the decontamination of polluted waters containing Pb^{2+} ions [12] and hydrocarbons [13]. To our knowledge, few biochars have already been tested as adsorbent materials of La, Nd and Dy [26,27] cations and the here investigated biochar of *Posidonia oceanica* is the first among those produced by seaweed biomasses.

The biochars were thoroughly characterized and the kinetics and thermodynamics of REEs recovery onto BCP, ABCP and BBCP were studied by means of batch experiments at different experimental conditions. The mechanism of REEs adsorption was hypothesized through the analysis of biochars characterization and through the parameter values of the most suitable kinetic and isotherm equations. Furthermore, the recyclability of biochar was tested through column experiments.

2. Experimental

2.1 Reagents

Phosphoric acid (Sigma Aldrich, 85.0%) and potassium hydroxide (Sigma Aldrich, 85.0%) solutions were used for BCP activation procedures.

REEs solutions were prepared by weighing the right amount of $La(NO_3)_3{\cdot}xH_2O$ (Sigma Aldrich, 32%–37% La), $Nd(NO_3)_3{\cdot}6H_2O$ (Sigma Aldrich, 32.0%–33.7% Nd) and $Dy(NO_3)_3{\cdot}xH_2O$ (Sigma Aldrich, 34%–37% Dy) salts. Sodium nitrate salt (Sigma Aldrich, 99.0%), used as ionic medium of REE ions solutions, was used after drying at 383.15 K for 2 h.

Nitric acid and sodium hydroxide used to adjust the pH of the metal ion solutions and in recycle experiments were prepared by diluting concentrated Sigma Aldrich and Fluka Analytical solutions. Ethylenediamine-*N*,*N*,*N*′,*N*′-tetraacetate (EDTA) solution, used to desorb the RE ions from ABCP in recycle experiments, was prepared by weighing the right amount of its disodium salt (Fluka, analytical grade).

Standard solutions of La^{3+}, Nd^{3+} and Dy^{3+} ions used in instrumental calibration were prepared by diluting 1000 mg/L standard solutions of the RE ions in 2% HNO_3 (CPAchem).
Certified buffer solutions at pH 4.01 and 7.00 (METTLER TOLEDO InLab® Solutions) were used to calibrate the pH-meter. All the solutions and suspensions were freshly prepared using CO_2 free ultra water ($\rho \geq 18$ MΩ·cm) and grade A glassware.

2.2 Biochar preparation and characterization

All the biochars used in this work were prepared from dead *Posidonia oceanica* leaves collected on the eastern Sicilian coasts as biomass. The BCP and BBCP were prepared following the procedures reported in the literature [13].
The ABCP was prepared by chemical activation of dried *Posidonia oceanica* leaves with H_3PO_4, according to the activation procedure reported in literature [28]. To this end, 20 g of dry raw material was stirred for 6 h in 300 mL of aqueous solution containing 41.28 mL of H_3PO_4 85% (*w*/*v*) at *T* = 358.15 K. Afterward, the solid product was filtered and dried in oven at 383.15 K for 12 h. The dried sample was then carbonized and activated in a fixed steel bed reactor at 748.15 K for 1 h with a heating rate of 7 K/min and under nitrogen flow of 160 mL/min. The produced biochar was washed with hot distilled water up to neutralization and dried in oven at 383.15 K for 12 h.
Both surface area and average pore size measurements of ABCP sample were carried out by analysis of N_2 adsorption-desorption isotherms at 77.35 K by using a Micromeritics ASAP 2020 instrument. The outgassing treatment was performed under a vacuum (667 Pa) at 523.15 K for 12 h. The surface area was determined by Brunauer-Emmett-Teller (BET) theory assuming that the coverage of nitrogen molecules was completed. Moreover, the pore size distribution was estimated by using the Barret-Joyner-Halenda (BJH) method during the desorption phase and density functional theory (DFT) method using nitrogen adsorption data, assuming a slit pore geometry.
Elemental analysis of ABCP was performed using a Thermo Fisher Scientific analyzer (model Flash EA 1112). In the experiment, ~2 mg of ABCP was examined in terms of carbon, hydrogen, nitrogen, sulfur, and oxygen (CHNS-O) content.
The morphology of the ABCP was studied by using a field emission scanning electron microscope (FE-SEM Philips model XL30 S FEG) equipped with a field emission gun and an EDX probe operating at an accelerating voltage of 20 kV.
Attenuated total reflection Fourier transform infrared (ATR-FTIR) spectra of the best REE adsorbent ABCP were acquired before and after the adsorption of the three REE cations on a Perkin-Elmer Frontier FT-IR/NIR spectrometer. The spectra were acquired in the 4000–400 cm^{-1} wavenumber range, with a spectral resolution of 16 cm^{-1}, and 100 scans; samples were dried for 24 h at 378.15 K and finely ground in an agate mortar before analysis.
The pH of point zero charge (pH_{pzc}) values of BCP, ABCP and BBCP were measured in $NaNO_3$ 0.1 mol/L. In details, 25 mg of each adsorbent was placed in different Erlenmeyer flasks containing 35 mL of $NaNO_3$ solution at different pH values in the range of 2–12. Purified N_2 gas was bubbled into each suspension for 10 min. After sealing with parafilm, the suspensions were magnetically stirred for 24 h. The pH of suspensions (final pH) was measured and plotted against the initial pH of the corresponding solutions (initial pH). The pH_{pzc} was obtained as the intersection with the blank curve. All the pH measurements were done with a pH-meter (GLP22 CRISON) equipped with a combined ISE–H^+ glass electrode (Ross type 8102) previously calibrated.

2.3 Procedures for equilibrium, kinetic and recycle experiments

The isotherm experiments of La^{3+}, Nd^{3+} and Dy^{3+} ions adsorption onto BCP, ABCP and BBCP were carried out in batch, at pH = 5.0 and at T = 298.15 K. Additional adsorption experiments (single batch or isotherms) with REE ions solutions at pH 3.0, 5.0 and 6.0 in $NaNO_3$ 0.1 mol/L were carried out with ABCP, which resulted in the best REE adsorbent among those investigated. In each isotherm experiment, varying biochar amounts (5–32 mg) were placed in 50 mL flasks containing 20 mL of the rare earth solution (c_{REE} = 0.07–0.58 mmol/L). The suspensions were shaken for 24 h using an orbital shaker (model M201-OR MPM Instruments srl), filtered through nylon syringe filters (SPHEROS, pore size = 0.45 μm), and the supernatants were collected for the pH and the equilibrium REE concentration (c_e) measurements. The reaching of adsorption equilibrium was verified through additional batch experiments in which the suspensions were filtered after 48 h.

Further batch experiments were carried out to study the kinetic of adsorption of the three RE ions onto the best adsorbent ABCP. Samples of *ca.* 9 mg of ABCP were placed in Erlenmeyer flasks containing 20 mL of REE solution (c_{REE} = 0.4 mmol/L), at pH = 5.0 and at T = 298.15 K. The suspensions were shaken and then filtered after different adsorbent-adsorbate contact time in the interval time of 2–1400 min. The collected supernatants were analyzed measuring their pH and the RE ions concentrations.

To test the reuse and recycling of ABCP, as well as the recovery of the three REE, *ca*. 17 mg of the adsorbent was packed into a glass column (diameter = 2 cm, length = 10 cm). Then, 15 mL of each REE solution ($c_{REE} \approx$ 0.4 mmol/L, pH = 5.0, T = 298.15 K) was flowed into the column at a flow rate of 6 mL/min for 16 h (the reaching of adsorption equilibrium was verified) by using a peristaltic pump (Gilson, Minipuls 3). The desorption step was carried out, after washing the adsorbent with 100 mL of distilled water, using 15 mL of, in turn, 0.1 mol/L HNO_3 or EDTA solutions at reflux for 6 h. After a further washing with 100 mL of distilled water, the next adsorption-desorption cycle began. Four adsorption/desorption cycles were carried out for each REE and extractant solution.

The RE ions concentrations of the solutions collected for the isotherm, kinetic and recycling experiments were determined by inductively coupled plasma optical emission spectroscopy (ICP-OES) technique by using a PerkinElmer Model Optima 2100, equipped with an auto sampler (model AS-90). The REE emission intensities were measured at the wavelengths of 398.852, 406.109 and 364.540 nm for La, Nd and Dy, respectively, and each measurement was repeated three times. Calibration curves were done in the same experimental conditions and covering the RE ions concentration range of adsorption experiments. The pH of the REE solutions, before and after contact with the adsorbents in the kinetic and isotherm experiments, was measured with a combined ISE–H^+ glass electrode (Ross type 8102) previously calibrated at the same experimental conditions. To this purpose, 25 mL of standardized HNO_3 solution was titrated with NaOH by using a potentiometric titration system (Metrohm, Model 888 Titrando) controlled by the TIAMO software.

2.4 Models for kinetic and isotherm studies of La^{3+}, Dy^{3+} and Nd^{3+} ions adsorption

Kinetic data of REE adsorption onto ABCP were tentatively subjected to regression analysis with several kinetic equations. Firstly, the pseudo-first order equation (PFO) of Lagergren [29] and the pseudo-second order equation (PSO) [30], the most common models in adsorption studies, were tested in the integrating nonlinear forms (boundary conditions: t = 0 to t = t and q_t = 0 and q_t = q_t) reported in Eqs. (1) and (2), respectively:

$$q_t = q_e\,(1 - e^{-k_1 t}) \quad (1)$$

$$q_t = \frac{q_e^2\, k_2\, t}{1 + q_e\, k_2 t} \quad (2)$$

where q_t and q_e are the adsorption capacity of the adsorbent material (mg/g) at time t and at the equilibrium; k_1 (min^{-1}) and k_2 (g·min/mmol) are the rate constants of adsorption.

Then, considering the heterogeneity of ABCP and the possible involvement of different functional groups during the RE ions binding, the following integrated forms of the Pseudo-*n*-order (PGO) model (Eq. (3)) [31] and of the double exponential model (DEM) (Eq. (4)) [32] were also tested:

$$q_t = q_e - \frac{q_e}{(k_n q_e^{(n-1)} t(n-1) + 1)^{\frac{1}{(n-1)}}} \quad (3)$$

$$q_t = q_e\,[1 - \alpha e^{-k_{D1} t} - (1 - \alpha) e^{-k_{D2} t}] \quad (4)$$

where k_n ((g/mmol)$^{n-1}$/min) and n are the rate constant and the general order of adsorption, respectively, k_{D1} and k_{D2} (min^{-1}) are the rate constants of the two adsorption stages hypothesized by DEM model and α accounts for the contribution of the two exponential terms to the overall adsorption process ($0 < \alpha < 1$).

The adsorption equilibrium data have been processed with Freundlich (Eq. (5)) [33] and Langmuir (Eq. (6)) [34] isotherm equations:

$$q_e = K_F\, c_e^{1/n} \quad (5)$$

$$q_e = \frac{q_m\, K_L\, c_e}{1 + K_L\, c_e} \quad (6)$$

where q_m (mmol/g) is the maximum adsorption ability of the adsorbent, c_e (mmol/L) is the REE concentration in solution at equilibrium; K_F (L$^{1/n}$·mmol$^{1-1/n}$/g) and K_L (L/mmol) are the Freundlich and Langmuir constants, respectively.

The adsorption ability at different contact time t (q_t, mmol/g) in kinetic experiments, or at equilibrium in the isotherm study (q_e, mmol/g) were calculated by Eq. (7):

$$q_t \text{ (or } q_e) = \frac{V\,(c_0 - c_t)}{m} \quad (7)$$

where V (L) is the volume of the REE solution in the batch and m is the mass of biochar (g); c_0 and c_t are the REE concentrations in the solutions (mmol/L) at $t = 0$ and $t = t$, respectively. At the equilibrium condition, c_t was replaced with c_e which is the REE concentration remaining in solution at the adsorption equilibrium.

3. Results and discussion

3.1 Biochars characterization

The results of the elemental analysis of ABCP are reported in Table 1 together with those of BCP and BBCP previously published [12,13]. Both the activation methods significantly impact the final properties of the BCP. Notably, acidic chemical activation resulted in a stronger carbonization compared to the basic activation as evidenced by the highest carbon content and the lowest O/C ratio of the ABCP sample.

Table 1. Results of elemental analysis (%)

Adsorbents	C	H	N	S	O	O/C	Reference
Posidonia oceanica	46.14	6.82	1.28	0.33	29.73	0.64	[12]
BCP	49.54	2.41	1.52	0.08	28.00	0.56	[12]
ABCP[a]	87.40	3.93	2.05	-	4.63	0.05	This work
BBCP	85.57	2.31	1.62	-	7.92	0.09	[13]

[a] Dry basis ±0.025

The main texture parameters relevant to the adsorption-desorption properties of BCP, ABCP, and BBCP samples are reported in Table 2. The N_2 adsorption-desorption profile for ABCP is depicted in Fig. 1 whilst those of BCP and BBCP, previously characterized, are reported in Refs. 12 and 13. The activation processes enhance the N_2 adsorption properties of ABCP and BBCP both in terms of specific surface area (324.194 and 650.8 m^2/g for ABCP and BBCP, respectively) and microporous surface area (266.469 and 484.85 m^2/g for ABCP and BBCP, respectively).

It is also noteworthy that the two activation methodologies change the pore volume, the microporous surface distribution, and the pore size distribution, as depicted in DFT graphs in Fig. 2. Although the biochar activated with H_3PO_4 exhibits a higher microporous surface area percentage (84.7%) compared to that activated with KOH (73.9%), the greater surface area of BBPC is justified by its higher pore volume (0.454 cm^3/g) compared to that of ABCP (0.0655 cm^3/g). The same rationale can be applied to the pore size distribution calculated by using the Barret-Joyner-Halenda (BJH) method (Table 3). Indeed, even though the distribution among micro, meso, and macro pores of ABCP and BBCP may appear similar to those of BCP, the difference lies precisely in the pore volume and in total area of each sample.

Table 2. Nitrogen adsorption–desorption measurements

Adsorbents	BCP[a]	ABCP	BBCP[c]
BET (m^2/g)	4.664	324.194 [b]	650.8
T-Plot micropore area (m^2/g)	2.378	266.469 [b]	484.85
$S_{micropore\ area}/S_{BET}$ (%)	51.0	84.7	73.9
Desorption average pore width (4 V/A) (nm)	12.905	2.706	2.791
Pore volume (cm^3/g)	0.0150	0.0655	0.454

[a] Ref. 12; [b] ±4.5%; [c] Ref. 13.

Figure 1. N_2 adsorption-desorption profile of ABCP

Figure 2. DFT pore size distribution of BCP, ABCP and BBCP

Table 3. Pore size percentage distributions of BCP, ABCP and BBCP

Adsorbents	BCP[a]		BBCP[b]		ABCP[c]	
	Area	Area distribution (%)	Area	Area distribution (%)	Area	Area distribution (%)

Micro (0–2 nm)	0.000	0.01	0.020	0.28	0.008	0.24
Meso (2–50 nm)	0.487	30.06	2.560	36.07	1.105	33.70
Macro (> 50 nm)	1.132	69.93	4.517	63.65	2.167	66.06
Total area	1.619	-	7.097	-	3.280	-

SEM-EDX experiments onto BCP and BBCP were discussed elsewhere [13]. Scanning electron micrographs of the ABCP at 1200× and 2000× magnifications are depicted in Fig. 3 together with EDX spectrum. The micrographs show that ABCP has a highly developed porosity as well as a rough unpattern surface composed of several discontinuities and cavities. These cavities are the result of the evaporation of H_3PO_4 molecules during the carbonization process which, leaving the previously occupied space, leads to the formation of a porous sponge-like material [35] with morphological characteristics completely different of that of BBCP [13]. Furthermore, a qualitative EDX analysis showed that ABCP contains phosphorus, low amounts of metals (Mg, Al and Si), and high carbon and oxygen quantities. In particular, the presence of phosphorus and the high oxygen content could be an indication of the presence of phosphate entities incorporated in the ABCP structure.

Figure 3. SEM micrographs at different magnifications (a, b) and EDX spectrum (c) of ABCP

Interesting insights regarding the possible interaction between the ABCP sorbent and the metal ions were achieved by ATR-FT-IR spectroscopy. The spectra of the carbonaceous material before and after adsorption are synoptically depicted in Fig. 4.

Figure 4. ATR-FT-IR spectra of ABCP before and after adsorption of La^{3+}, Dy^{3+} and Nd^{3+} ions.

All the spectra feature a shallow signal in the –OH stretching region (centered around 3350 cm^{-1}), which is scarcely diagnostic, indeed, because it might be attributed to both moisture traces and the hydroxyl groups possibly present in the materials. Rather, much more interesting information can be achieved by analysis of the double bond stretching and the fingerprint regions, in the wavenumber range of 1800–600 cm^{-1}. In this crowded spectral region, a superimposition of various bands can be envisaged, overlapped onto the well-known wide background adsorption band typical of carbonaceous graphene-like materials [36]. Signal attribution can be confidently put forward on the grounds of literature reports [37–42]. In details, the spectrum of the ABCP shows main signals centered at 1684 cm^{-1} (conjugated C=O str.), 1587 and 1416 cm^{-1} (C=C str.), 1071 and 945 cm^{-1} (phosphate), 877 and 734 cm^{-1} (C–H bend.). All these signals undergo remarkable modifications after adsorption of the three REE ions. In particular, the phosphate bands at 1071 and 945 cm^{-1} increase in intensity and undergo significantly different shifts for the three ions, moving up to 1050 and 1008 cm^{-1} with La^{3+}, 1082 and 1029 cm^{-1} with Dy^{3+}, and finally 1063 and 1013 cm^{-1} with Nd^{3+}, respectively. These findings unambiguously account for the occurrence of strong interactions between the hard Lewis acid cations and the phosphate groups. Besides, notable shifts to higher wavenumbers can be observed also for the other signals, even though no specific

cation effect can be observed. In particular, the conjugate carbonyl band moves up to 1700 cm^{-1}, which suggests a less effective electron back-donation from the aromatic graphene-like carbonaceous backbone. At the same time, this finding rules out any possible interaction between the carbonyl groups and the metal cation. Similarly, C=C stretching bands at 1587 and 1416 cm^{-1} move to 1605 and 1434 cm^{-1}, respectively, as well as C–H bending signals shift up to 897 and 750 cm^{-1}, respectively. The latter observation is in agreement with previous literature [38], and is consistent with the possible occurrence of relatively weak cation–π interaction with the carbonaceous backbone. Such an interaction may indeed decrease the overall electron density of the backbone (consistent with the carbonyl band shift), and possibly cause partial C=C bond localization.

The pH_{pzc} values of BCP, BBCP and ABCP in 0.1 mol/L $NaNO_3$ were found as large as 9.20, 6.15 and 4.10, respectively (see Fig. 5). Considering that at pH values lower than pH_{pzc} the adsorbent surface results positively charged, whereas the opposite occurs at pH > pH_{pzc}, at pH values close to 5 (as in the adsorption experiments), much more favorable electrostatic interactions are expected between the negatively charged ABCP and RE cations, in comparison to the positively charged BCP and BBCP.

Figure 5. pH_{pzc} of BCP, ABCP and BBCP in 0.1 mol/L $NaNO_3$.

3.2 Modelling of equilibria of La^{3+}, Nd^{3+} and Dy^{3+} ions adsorption by biochars

The adsorption equilibria of the two light rare earth ions La^{3+} and Nd^{3+} and of the heavy rare earth ion Dy^{3+} onto the BCP, BBCP and ABCP adsorbents were first studied in aqueous solutions at pH 5.0, at $I \rightarrow 0$ mol/L and T = 298.15 K.

The collected data (q_e vs c_e) were subjected to regression analysis by both the Langmuir and Freundlich isotherm equations. Results are depicted in Figs. 6 and 7 and in Figs. S1–S4 of the Supporting Materials together with the best fit curves of the two isotherm equations; the relevant fitting parameters are collected in Table 4.

As a preliminary observation, better fitting was achieved by means of the Langmuir model. Although the best fitting with a particular isotherm model does not necessarily give any indication on the uptake mechanism of the REE ions, the evaluation of the isotherm parameter values gives a very useful tool for predicting and optimize the sorption processes. Considering the q_m values, ABCP is the best adsorbent for the three cations among the three biochars investigated, followed by BBCP and BCP (see histogram reported in Fig. 8). The chemical activation processes improved the adsorption properties of BCP, in particular the acidic activation with H_3PO_4 (see section 2.2 for details). These findings are consistent with characterization results. Indeed, both activation processes increase the pore volume and the surface area of biochars. Moreover, ABCP showed the highest microporous surface area distribution (84.7%), followed by BBCP (73.9%). The largest adsorption capacity of ABCP is also enforced by the phosphate groups present in the microporous structure of the biochar, whose interaction with REE cations was evidenced by ATR-FT-IR spectra registered before and after REE ions adsorption. The adsorption performances of the three biochars mirror their pH_{pzc} values. In fact, the negatively charged surface of ABCP at pH = 5.0 promotes

the electrostatic interaction between the RE cations and the adsorbent. Conversely, at the same pH value, BCP and BBCP (see Fig. 5) have positive surface charge densities that hinder, and consequently reduce the REE adsorption. Both the maximum adsorption ability (q_m), and the affinity (K_L) trends of REE adsorption onto ABCP are: $Dy^{3+} > Nd^{3+} > La^{3+}$. This indicates that: (i) irrespective of the initial REE concentrations of solution to be treated, the adsorption ability trend of the same amount of ABCP at equilibrium (q_e) is the same of that of q_m; (ii) the adsorption capacity of ABCP towards REEs is inversely related to their ionic radius (ionic radii = 0.1045, 0.0983 and 0.0912 nm for La^{3+}, Nd^{3+} and Dy^{3+}, respectively) [43]. These findings agree with the hypothesized strong interactions between the hard Lewis acid REE ions and the phosphate groups present in the ABCP structure during adsorption.

The pH values of the REE-biochar suspensions of each isotherm experiment at adsorption equilibrium were measured and are reported in Table 4 (mean pH value of isotherm experimental points, pH_f). The pH_f values measured for ABCP, regardless of the REE ion, were fairly lower than the initial pH (~1.3 units). The REE adsorption onto BBCP caused a very small reduction of pH (~0.2 units). Finally, in the case of BCP, pH_f values rise by 0.5–1 unit compared to the initial pH. Considering that the REE ions form slightly soluble hydrolytic species $M(OH)_3$ at pH values higher than ~7 [44–46], the lowering of REE concentration in suspensions can be attributed exclusively to the adsorption process.

As it is clearly apparent from Fig. 5, the three biochars have different acid-base properties which can justify these pH variations observed during adsorption. The ABCP is the most acidic adsorbent, followed by the slightly acidic BBCP, whilst BCP behaves as a base. When the biochars are added to aqueous solution at pH = 5.0 containing also the REE ions, the ABCP causes a larger pH decrease than the one expected in water. The addition of BBCP does not change the pH at all, whereas the addition of BCP causes a lower increasing of pH than that expected in water. These observations can be reasonably explained by ion exchange between the REE cations and H^+ ions of binding sites of the biochars.

Being the apparently best REE adsorbent, the adsorption properties of ABCP were further investigated by carrying out isotherm experiments in 0.1 mol/L $NaNO_3$ at pH = 5.0 and single batch experiments at pH = 3.0 and 6.0 in the same ionic medium. The presence of an ionic medium decreases the adsorption ability of ABCP (Fig. 8). This may be explained by considering the shielding effect of the ions deriving from the salt dissociation, and the competition of the Na^+ ions, whose concentration is 5 orders of magnitude larger than the REEs. Moreover, the possible formation of ion pairs should be considered between nitrate ions and the trivalent REE cations which reduces the positive charge of the metal cations. These results are in agreement with those found by Qadeer et al. [46] who studied the effect of several cations and anions, including Na^+ and NO_3^- (1 g/L) on the adsorption of Dy^{3+} ions onto a commercial activated carbon. The authors found that Na^+ ions had a very small effect on the Dy^{3+} adsorption, whilst nitrate ions reduced the adsorption of ~ 30%.

A comparison of the q_e values calculated in 0.1 mol/L $NaNO_3$ at pH values of 3.0, 5.0 and 6.0 from batch experiments carried out at the same ABCP/REE ratio corresponding to an experimental point of the right side of Langmuir isotherms (where $q_e \rightarrow q_m$), was done to evaluate the pH effect on the adsorption process. A lowering of pH of two units (pH = 3.0) reduces the q_e by about one third, while, at pH = 6.0 the adsorption at equilibrium is almost the same (Fig. 8(b)). Once again, the q_e reduction with the decreasing pH can be ascribed to a cationic competition (in this case the proton) towards the binding groups of ABCP.

Literature q_m values of biochar and activated carbons recently used as adsorbents of the three REE cations are reported in Table S1 for useful comparisons. This table does not contain adsorption data calculated at pH values above 6.5 possibly affected by low soluble hydrolytic species of REE. To our knowledge, the ABCP is the best adsorbent of the three REE ions among the biochars (BC) present in literature[26,27]. Extending the comparison to activated carbons (AC) [44,47–55], only some commercial ACs [44,52–54] and few ACs obtained from pyrolysis of biomasses [47–51,55] showed higher recovery. In any case, being biochars the by-products of renewable fuel production, they should always be preferred because they are cheaper materials and fully respect the principles of the circular economy and environmental sustainability.

Table 4. Freundlich and Langmuir isotherm parameters for the La^{3+}, Nd^{3+} and Dy^{3+} ions adsorption onto biochars at pH = 5.0, without ionic medium ($I \rightarrow 0$ mol/L) or in 0.1 mol/L $NaNO_3$ and at T = 298.15 K.

Adsorbents	REE	Ionic medium	pH_f[a]	Langmuir model				Freundlich model			
				q_m (mmol/g)	K_L (L/mmol)	R^2	σ	K_F ($L^{1/n}\cdot mmol^{1-1/n}/g$)	N	R^2	σ
BCP	La^{3+}	-	5.52	0.074 ± 0.004	12.4 ± 2.6	0.9900	0.0021	0.077 ± 0.004	4.1 ± 0.7	0.9884	0.0023
BBCP		-	4.75	0.142 ± 0.004	71 ± 20	0.9879	0.0052	0.147 ± 0.007	14 ± 5	0.9779	0.0070
ABCP		-	3.71	0.23 ± 0.01	82 ± 20	0.9475	0.0180	0.28 ± 0.03	5 ± 1	0.8931	0.0257
ABCP		$NaNO_3$ [b]	4.04	0.154 ± 0.003	69 ± 9	0.9906	0.0048	0.19 ± 0.01	5.6 ± 0.9	0.9722	0.0083
ABCP		$NaNO_3$ (pH 3.0)	3.20	0.05 ± 0.01[c]	-	-	-	-	-	-	-
ABCP		$NaNO_3$ (pH 6.0)	3.60	0.15 ± 0.01[c]	-	-	-	-	-	-	-
BCP	Nd^{3+}	-	6.03	0.073 ± 0.005	7 ± 1	0.9930	0.0015	0.077 ± 0.007	2.6 ± 0.4	0.9867	0.0021
BBCP		-	4.83	0.111 ± 0.003	180 ± 88	0.9777	0.0057	0.118 ± 0.007	17 ± 9	0.9745	0.0061
ABCP		-	3.65	0.26 ± 0.01	68 ± 16	0.9530	0.0199	0.34 ± 0.04	5 ± 1	0.8575	0.0347
ABCP		$NaNO_3$ [b]	3.73	0.164 ± 0.007	87 ± 20	0.9525	0.0117	0.22 ± 0.01	4.8 ± 0.6	0.9714	0.0090
ABCP		$NaNO_3$ (pH 3.0)	3.50	0.04 ± 0.01[c]	-	-	-	-	-	-	-
ABCP		$NaNO_3$ (pH 6.0)	3.71	0.13 ± 0.01[c]	-	-	-	-	-	-	-
BCP	Dy^{3+}	-	6.13	0.072 ± 0.003	11 ± 1	0.9929	0.0017	0.08 ± 0.01	3.2 ± 0.4	0.9822	0.0026
BBCP		-	4.87	0.14 ± 0.01	96 ± 18	0.9896	0.0050	0.17 ± 0.01	7 ± 1	0.9856	0.0059
ABCP		-	3.69	0.31 ± 0.02	19 ± 4	0.9696	0.0174	0.45 ± 0.04	2.6 ± 0.3	0.9676	0.0178
ABCP		$NaNO_3$ [b]	3.63	0.15 ± 0.01	35 ± 7	0.9867	0.0047	0.18 ± 0.02	3.7 ± 0.8	0.9584	0.0082
ABCP		$NaNO_3$ (pH 3.0)	3.02	0.04 ± 0.01[c]	-	-	-	-	-	-	-
ABCP		$NaNO_3$ (pH 6.0)	3.39	0.12 ± 0.01[c]	-	-	-	-	-	-	-

[a] Mean pH value at adsorption equilibrium; [b] 0.1 mol/L; [c] q_e values from single batch experiments carried out at a ABCP:REE ratio corresponding to an experimental point of the right side of Langmuir isotherms ($q_e \rightarrow q_m$).

Figure 6. Adsorption isotherm of Nd^{3+} onto ABCP (□), BBCP (○) and BCP (△) in aqueous solutions at pH = 5 and T = 298.15 K. Experimental data were fitted to Freundlich (dashed lines) and Langmuir (continuous lines) models.

Figure 7. Adsorption isotherm of Nd^{3+} onto ABCP in aqueous solutions (□) and in 0.1 mol/L $NaNO_3$ (○) at pH = 5.0 and T = 298.15 K. Experimental data were fitted to Freundlich (dashed lines) and Langmuir (continuous lines) models.

Figure 8. (a) q_m values of REE adsorption onto BCP, BBCP and ABCP in aqueous solution at pH = 5; (b) q_e values of REE adsorption onto ABCP in $NaNO_3$, at pH = 3.0, 5.0 and 6.0 (experimental conditions: ~ 0.3 g of ABCP in 20 mL of aqueous solution containing 0.1 mol/L $NaNO_3$, c_{REE} = 0.3–0.4 mmol/L, at pH = 5.0 and T = 298.15 K).

3.3 Kinetics of La^{3+}, Nd^{3+} and Dy^{3+} adsorption onto biochars

The kinetics of La^{3+}, Nd^{3+} and Dy^{3+} adsorption onto ABCP, the best adsorbent among those investigated, were studied under the same experimental conditions, namely, ~9 mg of ABCP in 20 mL of REE solutions (c_{REE} = 0.4 mmol/L) at pH = 5.0, at $I \rightarrow 0$ mol/L and T = 298.15 K.

The data collected during kinetic experiments have been subjected to regression analysis by means of the PFO, PSO, PGO, and DEM equations (see the experimental section for details). The fitting parameters values, together with the statistical parameters of models fits (R^2 and σ), are reported in Table S2. First, the PFO and PSO kinetic models were used. The higher R^2 and the lower standard deviation (std. dev.) of fit obtained with PSO indicated a kinetic order higher than 1. However, the unsatisfactory goodness of fit of PSO along with visual observation of the experimental data plots (see kinetic data and fit curves of the four kinetic models depicted in Fig 9 and Figs. S5 and S6) suggested us testing also the PGO and the DEM equations as more suitable alternatives.

PGO model provides a non-predetermined adsorption order (n) [31,56,57] that could be suitable with ABCP adsorption. Indeed, as evinced from FT-IR spectra registered before and after REE adsorption, the activation process with H_3PO_4 created additional adsorption sites on the biochar surface that may cause a kinetic adsorption of REE whose order values could be higher than 2. However, the data fit with PGO model did not converge in the case of Dy^{3+}–ABCP system. Moreover, though the statistical outcomes of data fit of the other two REE–ABCP systems investigated were better than those obtained with the other kinetic models (see Table S2), the model parameters values were anomalously unreliable (e.g., n > 10 for the La^{3+} adsorption) and affected by large errors.

The heterogeneity of the ABCP surface could explain the poor fit of the tested kinetic models. At the same time, this heterogeneity makes the idea of more than a single contribution to REE adsorption kinetics reasonable. The best statistical outcomes (R^2 = 0.9778, 0.9912 and 0.9862 for Dy^{3+}, Nd^{3+} and La^{3+}, respectively) obtained with DEM model confirmed our idea.

Several forms of the DEM model have been proposed in literature for the kinetic studies of several adsorbent–adsorbate systems [32,58]. DEM model describes the REE uptake as a two-step process with parallel stages, one fast and one slow. Although no physical interpretation can be put forward

on the basis of model parameters values, the two steps may be hypothetically attributed to the existence of two main types of surface binding sites or two main parallel kinetic steps that involve diffusive processes. This last hypothesis could be linked to more or less accessible functional groups in the mesoporous structure of ABCP (pore volume = 0.0655 cm^3/g, average pore width = 2.706 nm).

Looking at DEM parameter values reported in Table 5, the comparison of k_{D1} and k_{D2} evidenced a superposition of a fast and a slow processes for all the REE ions adsorption. The contribution of these processes was quite similar for the three REE adsorptions (α = 0.36, 0.33 and 0.37 min^{-1} for Dy^{3+}, Nd^{3+} and La^{3+}, respectively) with the great part of REE ions adsorbed during the "fast" step. The values of kinetic constant k_{D2}, related to the "fast step" of process, were 0.59, 0.9 and 1.1 for La^{3+}, Dy^{3+} and Nd^{3+} ions, respectively. This k_{D2} trend could reflect the different sizes of the ions in solution and, therefore, their different diffusion coefficients. To the best of our knowledge, the hydrodynamic radii or diffusion coefficients of the three REE ions are not known but it is reasonable to hypothesize that they are related to the ionic radii whose values are 0.1045, 0.0983 and 0.0912 nm for La^{3+}, Nd^{3+} and Dy^{3+}, respectively [43]. This would explain the lowest k_{D2} value in the case of La^{3+} which has the largest ionic radius and reflects the dynamics of the interaction process between the RE ions that pass the diffusion layer and the surface of the adsorbent material. The k_{D1} value for each ion (0.005, 0.005 and 0.011 min^{-1} for La^{3+}, Dy^{3+} and Nd^{3+}, respectively) are instead specific for each ion not being mainly influenced by the diffusion process.

Table 5. Parameters of DEM kinetic equation for La^{3+}, Nd^{3+} and Dy^{3+} adsorptions onto ABCP at pH = 5.0, without the addition of ionic medium and at T = 298.15 K.

Metal ion	q_e (mmol/g)	α	k_{D1} (min^{-1})	k_{D2} (min^{-1})	R^2	σ^a
Dy^{3+}	0.329 ± 0.008[b]	0.36 ± 0.02	0.005 ± 0.001	0.9 ± 0.2	0.9778	0.0147
Nd^{3+}	0.282 ± 0.003	0.33 ± 0.02	0.011± 0.002	1.1 ± 0.2	0.9912	0.0068
La^{3+}	0.214 ± 0.005	0.37 ± 0.02	0.005 ± 0.001	0.54 ± 0.09	0.9862	0.0070

[a] ± std. dev. of fits; [b] ± std. dev.

Figure 9. Dependence of q_t (mg/g) on contact time for the Nd^{3+} ions adsorption onto ABCP. Data are fitted with PFO (dashed line) PSO (dotted line), PGO (dashed–dotted line), and DEM (continuous line) kinetic equations. Experimental conditions: 9 mg of ABCP; $I \rightarrow 0$ mol/L; $c_{Nd^{3+}}$= 0.4 mmol/L, pH = 5.0, T = 298.15 K.

3.4 Recycle and reuse of the ABCP adsorbent

Recycle and reuse experiments were carried out onto ABCP using 0.1 mol/L HNO_3 or EDTA as extractant solutions and doing four adsorption/desorption steps (see experimental for details) with both. The results are depicted in Fig. 10. The RE ions adsorption onto ABCP decreases ~80% after the first adsorption/desorption cycle with both extractant solutions, denoting scarce adsorbent recyclability. The best extractant solution was the 0.1 mol/L HNO_3. It was able to completely

desorb the REE cations in each of the four cycles probably through an ion exchange mechanism. The dramatic drop in the adsorption capacity occurred since the second cycle suggests that some significant structural alterations occur in the material after having interacted for the first time with the REE cations.

Figure 10. q_e values of adsorption/desorption steps for La^{3+} (top), Nd^{3+} (middle) and Dy^{3+} (bottom) onto ABCP. Experimental details: amount of ABCP ≈ 17 mg; REE ion solution: 15 mL, c_{REE} = 0.34–0.44 mmol/L, pH = 5.0 and T = 298.15 K; extractant solution: 15 mL of 0.1 mol/L EDTA (left histograms) or 0.1 mol/L HNO_3 (right histograms).

4. Conclusions

The aim of this work is to transform a biochar from the pyrolysis of dead leaves of *Posidonia oceanica* from a byproduct of a biofuel production process into a high value-added material. To this end, the pristine biochar (BCP) and its two forms chemically activated with H_3PO_4 (ABCP), and KOH (BBCP) were tested as adsorbent materials for the recovery of three rare earth cations, namely La^{3+}, Dy^{3+}, and Nd^{3+}. The adsorption abilities of biochars were studied from the kinetic and thermodynamic point of view subjecting the experimental adsorption data to regression analysis with several models. The results obtained can be summarized as follows:

(1) The chemical activation processes enhance the morphological characteristics of BCP, and reduce the pH_{pzc} value in the order of ABCP < BBCP < BCP. Moreover, the activation with phosphoric acid introduces phosphate groups in the biochar structure;

(2) The DEM model better describes the kinetic of REE cations recovery onto ABCP evidencing a superposition of a fast (k_{D2}) and a slow (k_{D1}) adsorption process with a quite similar contribution to the kinetics;

(3) The adsorption isotherms are well described by Langmuir equation. The BCP activation with KOH almost doubles its REE ions recovery ability. A more substantial improvement is achieved through the acidic activation with H_3PO_4. The highest q_m values of ABCP are mainly ascribed to the presence of phosphate groups in its structure. The REE recovery onto ABCP decreases in 0.1 mol/L $NaNO_3$ and increases with the decrease of their ionic radii, in agreement with the hypothesized strong interaction between hard Lewis acid REE ions and the phosphate groups in the ABCP structure;

(4) The recyclability tests on the ABCP do not give excellent results, evidencing an optimal REE adsorption and desorption only in the first of the four adsorption/desorption cycles and only with 0.1 mol/L HNO_3 as extractant solution. However, being the adsorbent a byproduct of biofuel production, it is a zero-cost material and in line with the principles of the circular economy and environmental sustainability.

Declaration of competing interest

The authors declare that they have no known competing financial interests or personal relationships that could have appeared to influence the work reported in this paper.

References

1. Dushyantha N, Batapola N, Ilankoon I, Rohitha S, Premasiri R, Abeysinghe B, et al. The story of rare earth elements (REEs): Occurrences, global distribution, genesis, geology, mineralogy and global production. *Ore Geol Rev*. 2020;122:103521.

2. Cardoso CE, Almeida JC, Lopes CB, Trindade T, Vale C, Pereira E. Recovery of rare earth elements by carbon-based nanomaterials – a review. *Nanomaterials*. 2019;9(6):814.

3. Balaram V. Rare earth elements: A review of applications, occurrence, exploration, analysis, recycling, and environmental impact. *Geosci Front*. 2019;10(4):1285.

4. Cheng S, Li W, Han Y, Sun Y, Gao P, Zhang X. Recent process developments in beneficiation and metallurgy of rare earths: A review. *J Rare Earths*. 2024;42(4):629.

5. Asadollahzadeh M, Torkaman R, Torab-Mostaedi M. Extraction and separation of rare earth elements by adsorption approaches: Current status and future trends. *Sep Purif Rev*. 2021;50(4):417.

6. Golev A, Scott M, Erskine PD, Ali SH, Ballantyne GR. Rare earths supply chains: Current status, constraints and opportunities. *Resour Policy*. 2014;41:52.

7. Geological Survey US. *Mineral Commodity Summaries 2024*. U.S. Geological Survey; 2024.

8. Kalantzakos S. The race for critical minerals in an era of geopolitical realignments. *Int Spect*. 2020;55(3):1.

9. EUR-Lex - 52023PC0160 - EN, document 2, ANNEX II.

10. Fujita Y, McCall SK, Ginosar D. Recycling rare earths: Perspectives and recent advances. *MRS Bull*. 2022;47(3):283.

11. Shanthi Bhavan J, Joy J, Pazhani A. Identification and recovery of rare earth elements from electronic waste: Material characterization and recovery strategies. *Mater Today Commun*. 2023;36:106921.

12. Cataldo S, Chiodo V, Crea F, Maisano S, Milea D, Pettignano A. Biochar from byproduct to high value added material – A new adsorbent for toxic metal ions removal from aqueous solutions. *J Mol Liq*. 2018;271:481.

13. Cataldo S, Muratore N, Giannici F, Bongiorno D, Chiodo V, Maisano S, et al. Hydrocarbons removal from synthetic bilge water by adsorption onto biochars of dead Posidonia oceanica. *Environ Sci Pollut Res*. 2022;29(60):90231.

14. Vieira MLG, Esquerdo VM, Nobre LR, Dotto GL, Pinto LAA. Glass beads coated with chitosan for the food azo dyes adsorption in a fixed bed column. *J Ind Eng Chem*. 2014;20(5):3387.

15. Fröhlich AC, Ocampo-Pérez R, Diaz-Blancas V, Salau NPG, Dotto GL. Three-dimensional mass transfer modeling of ibuprofen adsorption on activated carbon prepared by sonication. *Chem Eng J*. 2018;341:65.

16. Wang X, Cheng W, Xu R. Adsorption of rare earth elements on organic matter in coal. *J Rare Earths*. 2023;41(7):1108.

17. Zhao H, Luo H, Wu L, Zhou X, Zhang W, Li H, et al. Enhanced adsorption of Ce^{3+} from aqueous solutions by citric acid functionalized *Dicranopteris dichotoma*. *J Rare Earths*. Published online August 13, 2024. doi.org/10.1016/j.jre.2024.08.006.

18. Pereao O, Bode-Aluko C, Fatoba O, Laatikainen K, Petrik L. Rare earth elements removal techniques from water/wastewater: a review. *Desalin Water Treat*. 2018;130:71.

19. Royer-Lavallée A, Neculita CM, Coudert L. Removal and potential recovery of rare earth elements from mine water. *J Ind Eng Chem*. 2020;89:47.

20. Yaashikaa PR, Kumar PS, Varjani S, Saravanan A. A critical review on the biochar production techniques, characterization, stability and applications for circular bioeconomy. *Biotechnol Rep*. 2020;28:e00570.

21. Chiodo V, Zafarana G, Maisano S, Freni S, Urbani F. Pyrolysis of different biomass: Direct comparison among *Posidonia Oceanica*, *Lacustrine Alga* and *White-Pine*. *Fuel*. 2016;164:220.

22. Qiu B, Tao X, Wang H, Li W, Ding X, Chu H. Biochar as a low-cost adsorbent for aqueous heavy metal removal: A review. *J Anal Appl Pyrolysis*. 2021;155:105081.

23. Maisano S, Urbani F, Mondello N, Chiodo V. Catalytic pyrolysis of Mediterranean sea plant for bio-oil production. *Int J Hydrog Energy*. 2017;42(46):28082.

24. Telesca L, Belluscio A, Criscoli A, Ardizzone G, Apostolaki ET, Fraschetti S, et al. Seagrass meadows (*Posidonia oceanica*) distribution and trajectories of change. *Sci Rep*. 2015;5(1):12505.

25. Cantasano N. Deposition Dynamics of *Posidonia oceanica* "Banquettes" on Calabrian Sandy Beaches (Southern Italy). *Coasts*. 2021;1(1):25.

26. Kołodyńska D, Bąk J, Majdańska M, Fila D. Sorption of lanthanide ions on biochar composites. *J Rare Earths*. 2018;36(11):1212.

27. Ponou J, Wang LP, Dodbiba G, Matuo S, Okaya K, Fujita T. Recovery of dysprosium ions by biosorption-desorption onto organic plants wastes. *Int J Soc Mater Eng Resour*. 2014;20(2):141.

28. Yorgun S, Yıldız D. Preparation and characterization of activated carbons from Paulownia wood by chemical activation with H_3PO_4. *J Taiwan Inst Chem Eng*. 2015;53:122.

29. Lagergren SK. About the theory of so-called adsorption of soluble substances. *Sven Vetenskapsakad Handingarl*. 1898;24:1.

30. Blanchard G, Maunaye M, Martin G. Removal of heavy metals from waters by means of natural zeolites. *Water Res*. 1984;18(12):1501.

31. Tan KL, Hameed BH. Insight into the adsorption kinetics models for the removal of contaminants from aqueous solutions. *J Taiwan Inst Chem Eng*. 2017;74:25.

32. Cataldo S, Lo Meo P, Conte P, Di Vincenzo A, Milea D, Pettignano A. Evaluation of adsorption ability of cyclodextrin-calixarene nanosponges towards Pb^{2+} ion in aqueous solution. *Carbohydr Polym*. 2021;267:118151.

33. Freundlich HMF. Over the adsorption in solution. *J Phys Chem*. 1906;57:385.

34. Langmuir I. The adsorption of gases on plane surfaces of glass, mica and platinum. *J Am Chem Soc*. 1918;40(9):1361.

35. Daniel LS, Rahman A, Hamushembe MN, Kapolo P, Uahengo V, Jonnalagadda SB. The production of activated carbon from *Acacia erioloba* seedpods via phosphoric acid activation method for the removal of methylene blue from water. *Bioresour Technol Rep*. 2023;23:101568.

36. Di Vincenzo A, Chillura Martino D, Piacenza E, Conte P, Pettignano A, Lazzara G, et al. Reduced graphene oxide/silver nanoparticles/β-cyclodextrin nanosponges composites with improved photocatalytic activity. *Appl Surf Sci Adv*. 2023;15:100407.

37. Trivedi MK, Branton A, Trivedi D, Nayak G, Bairwa K, Jana S. Physicochemical and Spectroscopic Characterization of Biofield Treated Triphenyl Phosphate. *Am J Appl Chem*. 2015;3(5):168.

38. Dai X, Thi Hong Nhung N, Hamza MF, Guo Y, Chen L, He C, et al. Selective adsorption and recovery of scandium from red mud leachate by using phosphoric acid pre-treated pitaya peel biochar. *Sep Purif Technol*. 2022;292:121043.

39. Guo H, Ma L, Shen F, Yang G, Zhang Y, Deng S, et al. Effects of La-involvement on biomass pyrolysis behaviors and properties of produced biochar. *J Rare Earths*. 2017;35(6):593.

40. Janu R, Mrlik V, Ribitsch D, Hofman J, Sedláček P, Bielská L, et al. Biochar surface functional groups as affected by biomass feedstock, biochar composition and pyrolysis temperature. *Carbon Resour Convers*. 2021;4:36.

41. Jetsrisuparb K, Jeejaila T, Saengthip C, Kasemsiri P, Ngernyen Y, Chindaprasirt P, et al. Tailoring the phosphorus release from biochar-based fertilizers: role of magnesium or calcium addition during co-pyrolysis. *RSC Adv*. 2022;12(47):30539.

42. Zhang Z, Liu B, He Z, Pan P, Wu L, Lin B, et al. The Synergistic Effect of Biochar-Combined Activated Phosphate Rock Treatments in Typical Vegetables in Tropical Sandy Soil: Results from Nutrition Supply and the Immobilization of Toxic Metals. *Int J Environ Res Public Health*. 2022;19(11):6431.

43. Lide DR, ed. *CRC Handbook of Chemistry and Physics, 83rd Edition*. Boca Raton: CRC Press; 2002.

44. Babu CM, Binnemans K, Roosen J. Ethylenediaminetriacetic acid-functionalized activated carbon for the adsorption of rare earths from aqueous solutions. *Ind Eng Chem Res*. 2018;57(5):1487.

45. Dasgupta K, Vijayalakshmi R, Anitha M. Recovery of Nd (III) in coexistence with Fe (III) ions from aqueous phase using functionalized multiwalled carbon nanotubes: an environmental benign approach. *J Environ Chem Eng*. 2016;4(2):2103.

46. Qadeer R, Hanif J. Adsorption of dysprosium ions on activated charcoal from aqueous solutions. *Carbon*. 1995;33(2):215.

47. El-Aryan YF, Melhi S, Alosaimi EidH, Alqahtany FZ, Zaher WF. Kinetic and Isothermal Study for Adsorption of Lanthanum on Modified Activated Carbon. *Russ J Phys Chem A.* 2023;97(14):3379.

48. El-Aryan YF, Melhi S, Ahmed IM, El-Ossaily YA, Ali HM, El-Gammal B, et al. Exploring the adsorption potential of lanthanum (III), samarium (III), and cerium (III) from aqueous solutions utilizing activated carbon derived from date seeds. *Inorg Chem Commun*. 2024;163:112331.

49. Pinheiro RF, Grimm A, da Boit Martinello K, Khan MR, Ahmad N, Silva LFO, et al. Vine pruning waste-based activated carbon for cerium and lanthanum adsorption from water and real leachate. *J Rare Earths*. 2024;42(10):1960.

50. Pinheiro RF, Grimm A, Oliveira MLS, Vieillard J, Silva LFO, De Brum IAS, et al. Adsorptive behavior of the rare earth elements Ce and La on a soybean pod derived activated carbon: Application in synthetic solutions, real leachate and mechanistic insights by statistical physics modeling. *Chem Eng J*. 2023;471:144484.

51. Awwad NS, Gad HMH, Ahmad MI, Aly HF. Sorption of lanthanum and erbium from aqueous solution by activated carbon prepared from rice husk. *Colloids Surf B Biointerfaces*. 2010;81(2):593.

52. Marwani HM, Albishri HM, Jalal TA, Soliman EM. Study of isotherm and kinetic models of lanthanum adsorption on activated carbon loaded with recently synthesized Schiff's base. *Arab J Chem*. 2017;10:S1032.

53. Iannicelli-Zubiani EM, Stampino PG, Cristiani C, Dotelli G. Enhanced lanthanum adsorption by amine modified activated carbon. *Chem Eng J*. 2018;341:75.

54. Qadeer R. Adsorption of neodymium ions on activated charcoal from aqeous solutions. *J Radioanal Nucl Chem*. 2005;265(3):377.

55. Alcaraz L, Escudero ME, Alguacil FJ, Llorente I, Urbieta A, Fernández P, et al. Dysprosium removal from water using active carbons obtained from spent coffee ground. *Nanomaterials*. 2019;9(10):1372.

56. Cazalbou S, Bertrand G, Drouet C. Tetracycline-loaded biomimetic apatite: an adsorption study. *J Phys Chem B*. 2015;119(7):3014.

57. Largitte L, Pasquier R. A review of the kinetics adsorption models and their application to the adsorption of lead by an activated carbon. *Chem Eng Res Des*. 2016;109:495.

58. Chiron N, Guilet R, Deydier E. Adsorption of Cu(II) and Pb(II) onto a grafted silica: isotherms and kinetic models. *Water Res*. 2003;37(13):3079.

Graphical abstract

Synthetic representation in steps of the use of adsorbent material obtained from dead *Posidonia oceanica* leaves for the adsorption and subsequent recovery of rare earths ions.

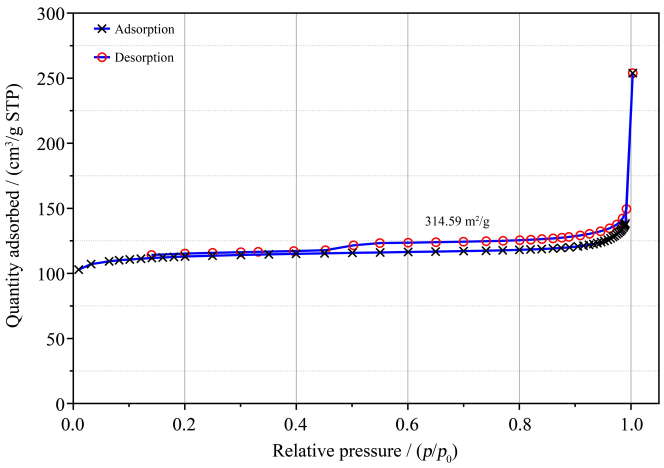

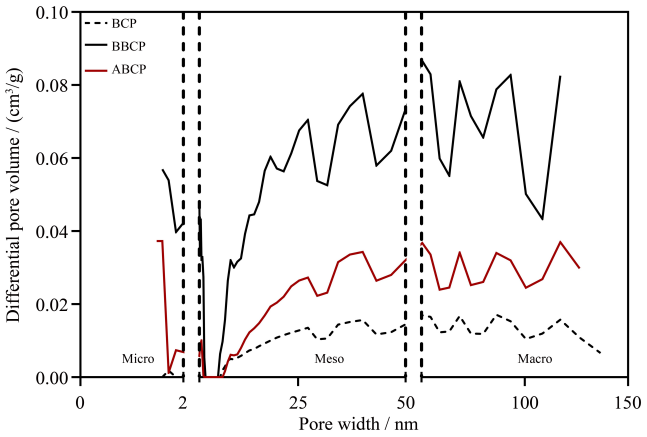

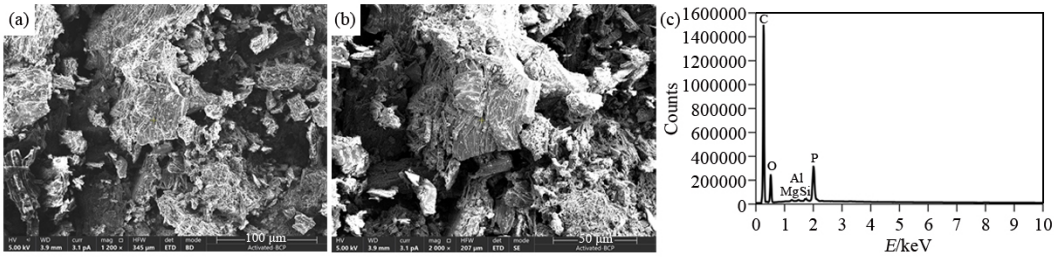

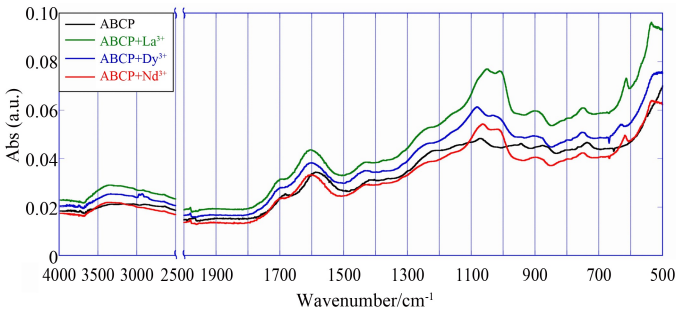

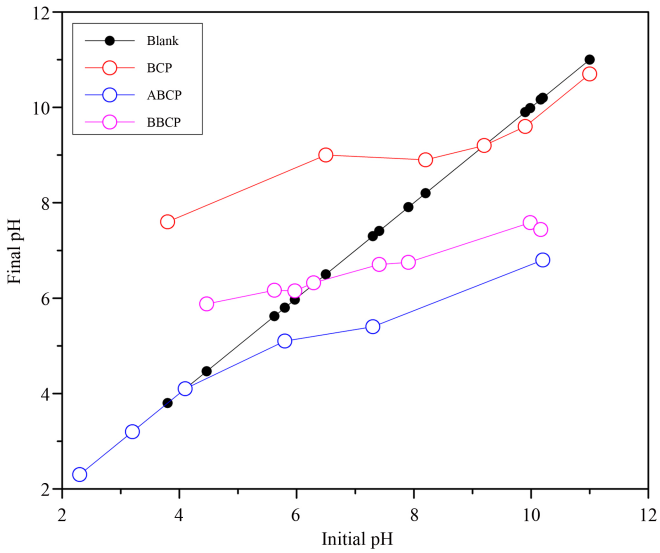

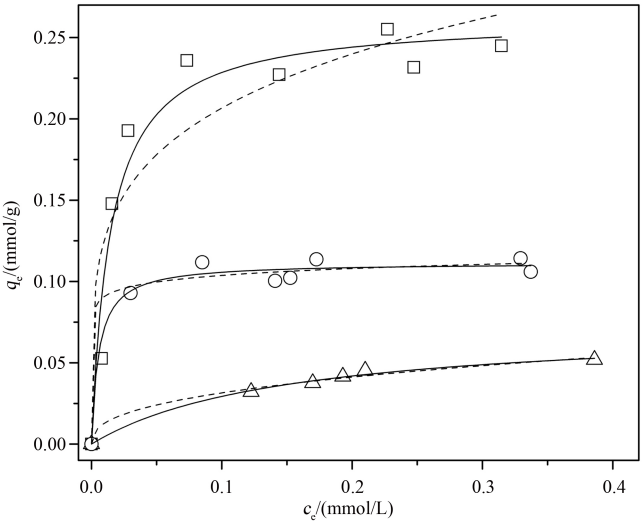

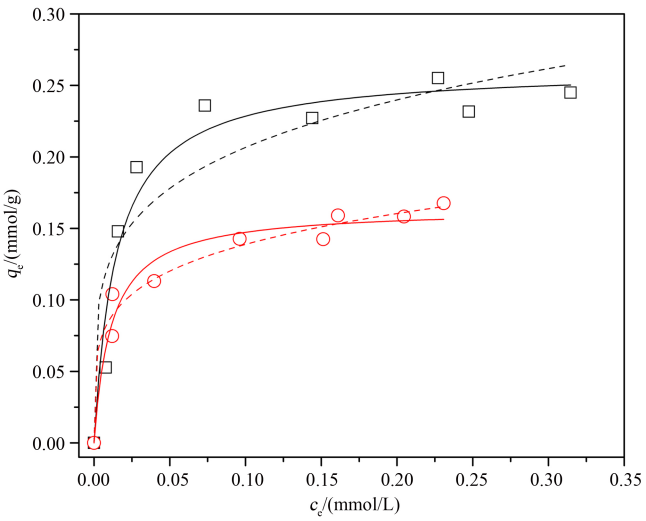

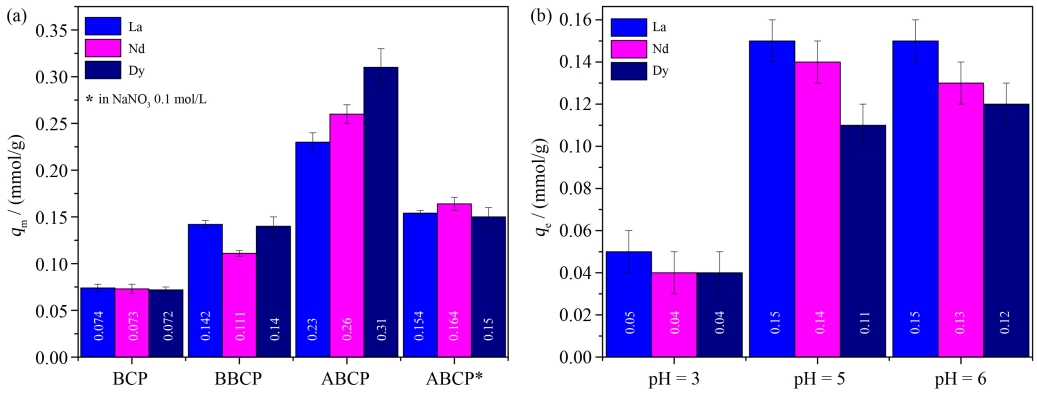

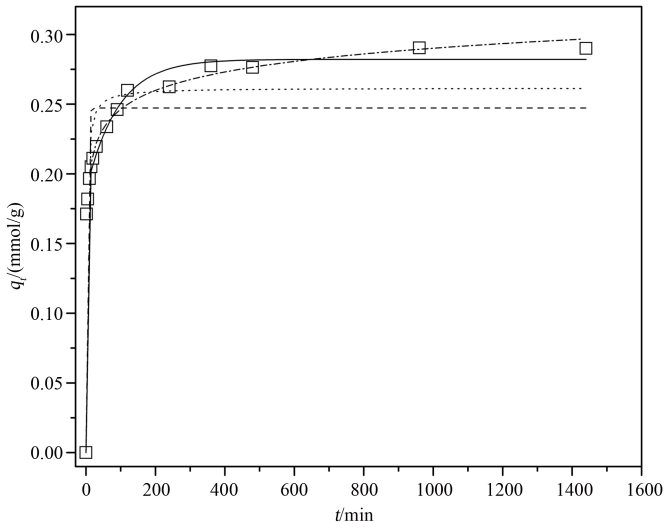

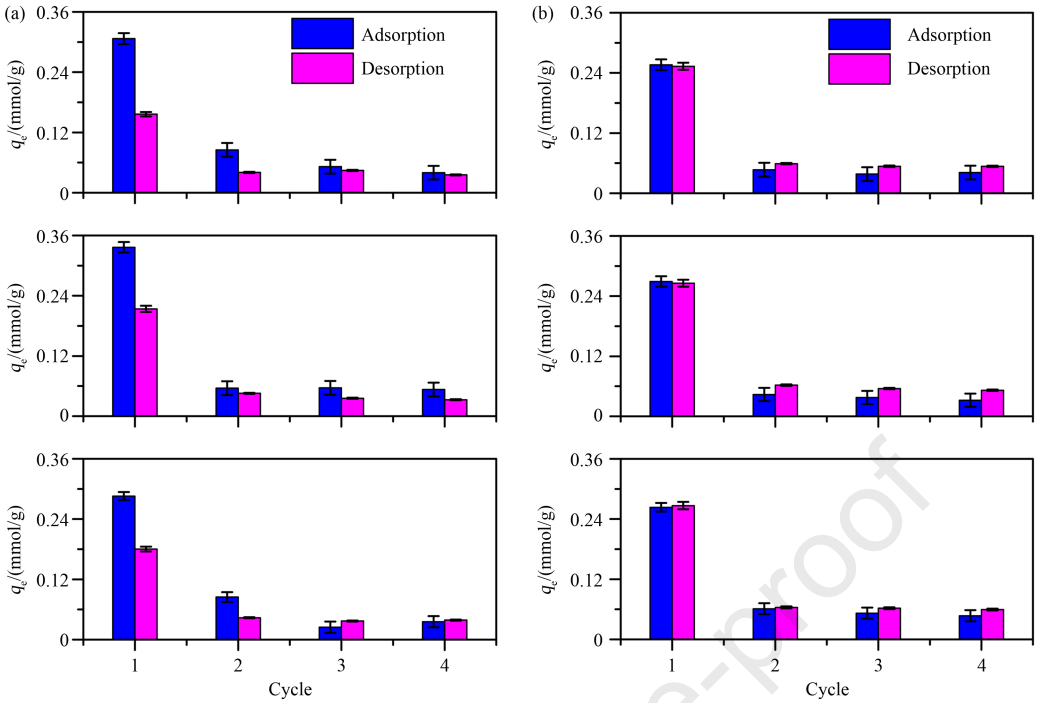

Highlights

- Biochars of dead *Posidonia oceanica* leaves were used as adsorbents of rare earth ions;
- Adsorbent materials have been extensively characterized;
- Chemically activated biochars showed better recovery ability than pristine biochar;
- kinetic and isotherm adsorption data were processed with different models;
- the effects of pH and ionic medium on the REE adsorption were evaluated.

Declaration of interests

☒ The authors declare that they have no known competing financial interests or personal relationships that could have appeared to influence the work reported in this paper.

☐ The author is an Editorial Board Member/Editor-in-Chief/Associate Editor/Guest Editor for *[Journal name]* and was not involved in the editorial review or the decision to publish this article.

☐ The authors declare the following financial interests/personal relationships which may be considered as potential competing interests: